International Journal for Parasitology 49 (2019) 963–973

Contents lists available at ScienceDirect

International Journal for Parasitology

journal homepage: www.elsevier.com/locate/ijpara

Inhibition of *Opisthorchis felineus* glutathione-dependent prostaglandin synthase by resveratrol correlates with attenuation of cholangiocyte neoplasia in a hamster model of opisthorchiasis

Maria Y. Pakharukova [a,b,*], Oxana G. Zaparina [a], Anna V. Kovner [a], Viatcheslav A. Mordvinov [a]

[a] Laboratory of Molecular Mechanisms of Pathological Processes, Institute of Cytology and Genetics, Siberian Branch of Russian Academy of Sciences, 10 Lavrentiev Ave., Novosibirsk 630090, Russia
[b] Department of Natural Sciences, Novosibirsk State University, 2 Pirogova Str., Novosibirsk 630090, Russia

ARTICLE INFO

Article history:
Received 15 April 2019
Received in revised form 4 July 2019
Accepted 10 July 2019
Available online 16 October 2019

Keywords:
Foodborne trematodes
Opisthorchiasis
Opisthorchis felineus
Chronic inflammation
High-grade biliary neoplasia
Resveratrol
Animal model

ABSTRACT

Food-borne trematodiases represent major neglected parasitic diseases. Trematodes of the family Opisthorchiidae including *Opisthorchis felineus*, *Opisthorchis viverrini* and *Clonorchis sinensis* are ranked eight on the global list of the 24 most prevalent food-borne parasites. Chronic *O. felineus* infection symptoms include precancerous lesions with the potential for malignancy. In recent decades, liver flukes of the family Opisthorchiidae have been extensively scientifically explored, however despite this the molecular mechanisms of *O. felineus* pathogenicity and its carcinogenic potential have not been studied. *Opisthorchis felineus* glutathione-dependent prostaglandin synthase (GST σ) is the major component of the excretory–secretory product of this liver fluke. We hypothesised that the activity of this enzyme is involved in the infection pathogenesis, including the formation of precancerous lesions. To test this hypothesis and to gain insights into the mechanisms of precancerous lesion formation, we (i) investigated whether excretory parasitic GST σ retains its enzymatic activity, (ii) tested resveratrol (RSV) as a possible inhibitor of this enzyme, and (iii) assessed biliary neoplasia and oxidative DNA damage as well as the expression of neoplasia and fibrogenesis marker genes after prolonged administration of RSV in a hamster model. RSV was found to inhibit GST σ enzymatic activity in a dose-dependent manner ($R = 0.85$, $P < 0.001$; half-maximal effective dose (ED_{50}) = 48.6 μM). Prolonged administration of RSV significantly suppressed high-grade biliary neoplasia ($P = 0.008$), attenuated upregulation of hyperplasia and fibrogenesis-related genes (*Tgfb*, *α-SMA* and *CK7*), and decreased the elevated oxidative DNA damage. Taking into account that RSV can influence a wide range of pathways, further research is needed to confirm the role of GST σ in *O. felineus* pathogenicity. Nevertheless, the chemopreventive effect of RSV targeting biliary neoplasia formation might be useful for improving the outcomes in infected populations and represents a compelling rationale for RSV testing in combination chemotherapy of opisthorchiasis.

1. Introduction

The fish-borne liver fluke *Opisthorchis felineus* (Rivolta, 1884) is the causative agent of opisthorchiasis felinea across a vast territory that spans regions of Eurasia (Armignacco et al., 2013; Pakharukova and Mordvinov, 2016). Trematodes of the family Opisthorchiidae are ranked eighth on the global list of 24 most prevalent food-borne parasites (WHO, 2014). Two species, the liver flukes *Opisthorchis viverrini* (Poirier, 1886) and *Clonorchis sinensis* (Loos, 1907) (Sripa et al., 2007) were classified as Group 1 biological carcinogens and a major risk factor of cholangiocarcinoma (CCA) in endemic areas (Sripa et al., 2007).

Recently, we presented findings that support the inclusion of *O. felineus* in Group 1 of biological carcinogens (Gouveia et al., 2017; Maksimova et al., 2017; Pakharukova et al., 2019a). The histological manifestations of chronic infection with these liver flukes (Sripa et al., 2007; Maksimova et al., 2017) include inflammation with dysplasia; gallbladder dysfunction; severe fibrosis; biliary intraepithelial neoplasia of grades I, II, and III; and other precancerous lesions able to progress to malignancy (Gouveia et al., 2017). Although the biology and host–parasite relationship of this trematode are similar to those of other carcinogenic flukes (*O. viverrini* and *C. sinensis*), the molecular mechanisms of *O. felineus* pathogenicity and the carcinogenic potential have not been well

* Corresponding author at: 10 Lavrentiev Ave., Novosibirsk 630090, Russia.
E-mail address: pmaria@yandex.ru (M.Y. Pakharukova).

https://doi.org/10.1016/j.ijpara.2019.07.002
0020-7519/

studied (Pakharukova and Mordvinov, 2016; Pakharukova et al., 2019a), and hypotheses are based only on the data obtained from other species, in particular *O. viverrini* and *C. sinensis*. It is believed that *O. felineus* infection–associated tumorigenesis is based on cellular DNA damage and chronic inflammation (Sripa et al., 2012, 2018; Yongvanit et al., 2012). In addition, the carcinogenic potential is attributed to the effects of proteins and metabolites secreted by liver flukes (Sripa et al., 2012; Correia da Costa et al., 2014; Chaiyadet et al., 2015).

The major component of the *O. felineus* excretory–secretory product is glutathione-dependent prostaglandin synthase (also known as glutathione S-transferase (GST) σ) (Lvova et al., 2014). This parasitic enzyme may participate in chronic inflammation by contributing to the production of prostanoids (Sommer et al., 2003) as shown for the extracellular GST1 of *Onchocerca volvulus* (Sommer et al., 2003). The *GST-σ* gene in adult worms is among the 10 most abundant genes (GenBank accession no: GBJA01007477.1) (Pomaznoy et al., 2016; Ershov et al., 2019). Nevertheless, the role of this enzyme (produced in large amounts and secreted into the surrounding space (Lvova et al., 2014)) in the mechanisms of the host–parasite relationship is unknown. We hypothesised that GST-σ may contribute to oxidative stress and the pathogenicity of *O. felineus*. To test this idea, it was necessary to find an effective GST inhibitor acting in vivo. We supposed that resveratrol (RSV) could be such an inhibitor.

RSV is a stilbene polyphenol present in various plant species including berries, grapes, and peanuts (Baur and Sinclair, 2006). It has antioxidant and cardioprotective properties and therapeutic effects on atherosclerosis, diabetes, muscular dystrophy (Baur and Sinclair, 2006), and cancer (Jang et al., 1997). RSV reduces the formation of mutagenic oxysterols and oestrogen–DNA adducts (Cavalieri and Rogan, 2010).

Thus, to elucidate the carcinogenic potential of trematodes and to gain first insights into the mechanisms of precancerous lesion formation associated with *O. felineus* infection, the objectives of this study were (i) to investigate whether secreted parasitic GST-σ retains its enzymatic activity; (ii) to test RSV as a possible inhibitor of this enzyme; (iii) to assess biliary neoplasia and oxidative DNA damage as well as the expression of hyperplasia and fibrogenesis marker genes after prolonged administration of RSV in a hamster model of opisthorchiasis felinea.

2. Materials and methods

2.1. Ethics statement

All the procedures were in compliance with European Union Directive 2010/63/EU for animal experiments. The animals were kept and treated according to the protocols approved by the Committee on the Ethics of Animal Experiments at the Institute of Cytology and Genetics, the Siberian Branch of the Russian Academy of Sciences, Russia (ICG SB RAS; Permit Number: 42 of 25.05.2018).

2.2. Animals and infection

Syrian hamsters (*Mesocricetus auratus*) were purchased from the Animal Facility of the ICG SB RAS. Euthanasia was implemented via carbon dioxide inhalation, and every effort was made to minimise the suffering of the hamsters. *Opisthorchis felineus* metacercariae were collected from naturally infected fish (*Leuciscus idus*) caught in the Ob River near Novosibirsk (Western Siberia) and were extracted as described previously (Pakharukova et al., 2018, 2019b,c). Briefly, the fish tissue was immersed in a digestion solution (0.9% NaCl in distilled water with 1% pepsin and 1% HCl, pH 2.0) for 2 h at 37 °C followed by filtration. After several washes with normal saline, the metacercariae were collected and identified under a light microscope.

To assess the influence of oral RSV (Sigma–Aldrich, USA) administration (for 1 or 3 months) on progression of opisthorchiasis-associated pathologies, 37 2-month-old male hamsters (*M. auratus)* were randomly subdivided into four groups: I, uninfected; II, RSV alone (1 mg/kg of RSV administered (with food)); III, OF (infected with 75 metacercariae of *O. felineus*; and IV, OF + RSV (infected with 75 metacercariae of *O. felineus* and 1 mg/kg of RSV administered (with food)). The hamsters were housed, one per cage, under conventional conditions and were provided with standard rodent feed (PK-120–1; Laboratorsnab, Ltd., Moscow, Russia) and water ad libitum. RSV was dissolved in ethanol (Sigma–Aldrich, USA) to prepare an 88 mg/mL solution. Before oral administration, it was diluted with PBS (pH 6.11) to a final concentration of 5 mg/mL.

The hamsters of groups III and IV were infected with 75 metacercariae per os via oral gavage. The dose of RSV was selected according to previously published data (Girbovan and Plamondon, 2015). Groups I and III (which did not receive RSV) consumed the control diet with the addition of dried bread slices, and the other groups consumed the same diet supplemented with RSV (1 mg/kg of body weight) on the dried bread slices. Each hamster in the treatment group received RSV daily. The animals received RSV starting from the first day of infection. The total duration of the experiment was 3 months. Four hamsters from the uninfected group and 4–7 hamsters from each of the other groups were euthanised and necropsied at 1 and 3 months p.i.

2.3. Sample collection and histopathological analysis

Hamsters were euthanised using carbon dioxide, after which blood was collected by cardiac puncture. Blood was centrifuged at 3000*g* for 20 min at 4 °C to obtain serum. Urine was collected by bladder puncture. The serum and urine samples were aliquoted and stored at −80 °C. The liver was carefully dissected and placed in 10% buffered formalin (Biovitrum, Russia). After fixation for 3 days, the specimens were dehydrated in a graded series of ethanol solutions and then absolute ethanol, cleared in xylene, and soaked in melted paraffin. After that, we embedded the specimens in paraffin using Microm (Microm, UK). Four-μm-thick sections were prepared by means of a microtome.

For histopathological analysis, the tissue sections were stained with H&E or Van Gieson's stain (Supplementary Fig. S1) by standard methods and examined under a light microscope (Axioskop 2 Plus; Zeiss, Germany). Histological features of liver including inflammatory cell infiltration, cholangiocyte hyperplasia, bile duct dysplasia, periductal fibrosis, and bile duct cell proliferation were manually scored by two independent investigators and a senior pathologist confirmed the score. A scoring method of type Ratio (morphometry) of data measurements was applied (Gibson-Corley et al., 2013; Maksimova et al., 2017). This method is based on counting several fields of tissue (e.g. 10 random 400× fields) for each animal, each field is scored and a mean score assigned for the whole tissue of that animal (Gibson-Corley et al., 2013). This method is a good alternative for a grading system based on severity for the feature or disorder of interest to overcome low reproducibility of such grading and staging systems (Klopfleisch, 2013). Briefly, histological changes were assessed in two lobes of the liver of each animal. Each section of a lobe was analysed in all fields of view (20–30 fields). Each field of view was divided into 100 squares in Morphometry software. Inflammatory cell infiltration, cholangiocyte hyperplasia, bile duct dysplasia, periductal fibrosis, and bile duct cell proliferation were assessed by means of a percentage of the area (the number of squares occupied). Metaplasia of the epithelium was assessed via the number of

metaplastic cells in a field of view. Detailed data are presented in Supplementary Table S1. The data were expressed as a percentage of the maximum possible score and presented as a heat map using the heatmap.2 (v.2.38) R package. For immunohistochemistry 4 μm thick sections were prepared by means of a microtome. Staining was performed using the rabbit antiserum against recombinant *O. felineus* GST sigma (1:20) (Razumov et al., 2016), followed by probing with the secondary horseradish peroxidase–conjugated antibodies (Abcam, USA). The sections were coverslipped with Fluoro-shield mounting medium containing DAPI (cat. # F6057, Sigma-Aldrich, USA) and visualised under an AxioImager A1 microscope (Zeiss) with camera AxioCam MRc (Zeiss).

2.4. Serum biochemistry

Aspartate aminotransferase (AST), alanine aminotransferase (ALT), total bilirubin, total cholesterol, creatinine, and urea were quantified in blood serum samples with the corresponding kits (Vector-Best, Russia).

2.5. 8-Hydroxy-2′-deoxyguanosine (8OH-dG) level

Urinary 8-hydroxy-2′-deoxyguanosine (8OH-dG) concentration was measured using the 8OH-dG ELISA kit (cat. # ab201734, Abcam).

2.6. Primer design

Sequences for all primers and probes can be found in Supplementary Table S2 (Synthol, Russia).

2.7. Total-RNA extraction, cDNA synthesis, and real-time PCR

Total RNA for real-time PCR was isolated from flukes using the Aurum total RNA extraction kit (Bio-Rad, USA). Concentrations of RNA were determined on a NanoDrop spectrophotometer (ND1000, NanoDrop Technologies, USA). First-strand cDNA synthesis was performed with the RevertAid Kit (Fermentas, European Union). Expression levels of the genes were measured by real-time PCR involving the EVA Green Reagent Mix (Synthol, Russia) on a CFX96 real-time PCR system (Bio-Rad, USA). As an endogenous internal control for normalisation, we chose *Gapdh* (between *Gapdh* and *Hprt1*) because this gene has a lower M-value ($M < 1.0$; Bio-Rad). Various investigators have defined $M < 1.0$ as an acceptable criterion for selection of reference genes for reverse-transcription PCR (RT-PCR) (Strube et al., 2008). Triplicate real-time PCRs were performed on each sample. The fold-change in target gene expression (that was normalised to the control) was calculated from threshold cycle values (C_t; CFX96 software).

2.8. Western blotting

Immunoblotting was performed as described elsewhere (Xiao et al., 2016; Petrenko et al., 2017). Antibodies and dilutions used in this study include anti-β-actin (1:2000; cat. # ab8226, Abcam), anti-smooth muscle actin α (1:2000; cat. # ab7817, Abcam), anti-cytokeratin 7 (1:2000; cat. # ab9021, Abcam), anti-E-cadherin (1:2000; cat. # ab76055, Abcam), and anti-PCNA (1:2000; cat. # 2139540, Sony) antibodies. Quantitative densitometric analyses were performed on digitised images of immunoblots in the Quantity One software (Bio-Rad, USA).

2.9. Preparation of the incubation medium and worm lysates, and a GST σ activity assay

For preparation of the incubation medium, adult worms were recovered from the livers of hamsters infected 1 and 3 months earlier, and then the worms were thoroughly washed with sterile saline (0.9% NaCl). The worms were incubated at 37 °C for 24 h in the RPMI 1640 medium (Life Technologies, USA) supplemented with 100 U/ml of penicillin, 0.1 μg/ml of streptomycin, 0.25 μg/ml of amphotericin B (Sigma–Aldrich, USA), and 1% of glucose in a CO_2 incubator (Mordvinov et al., 2017; Pakharukova et al., 2018, 2019b). After 24 h of incubation, the worms were removed from the medium and were subjected to lysate preparation. A protease inhibitor cocktail (Amresco, USA) was added to the worm incubation medium. The incubation medium from each group was centrifuged (for 20 min at 12,000*g* and 4 °C), aliquoted, and stored at −80 °C.

For lysate preparation, 5 mg of worm tissue were dissected, placed in tubes, and homogenised in 0.3 mL of cold lysis buffer (150 mM NaCl, 1.0% of NP-40, 50 mM Tris-HCl pH 8.0, and 0.2 mM phenylmethylsulfonyl fluoride). Constant agitation of samples was maintained for 2 h at 4 °C. Then, the samples were centrifuged (for 20 min at 12,000*g* and 4 °C), and the supernatant was aspirated and placed in a fresh tube kept on ice. The protease inhibitor cocktail (Amresco) was added to the samples. The lysates were aliquoted and stored at −80 °C. The protein concentration was determined with a Bicinchoninic Acid Assay (BCA) Kit (Thermo Fisher Scientific, USA).

The GST assay was conducted in 1 cm cuvettes as described previously (Mazari et al., 2015) using adult worm lysates and worm incubation media. The reaction mixture consisted of 1.0 mmol of 1-fluoro-2,4-dinitrobenzene (Sigma, USA), 1.0 mmol of glutathione (GSH, Sigma, USA), and 5–25 μl of a worm lysate or worm incubation medium (1–10 mg of protein) in a final volume of 0.5 ml. The reaction was initiated with glutathione addition, vortexing, and 15 s equilibration prior to recording of absorbance changes. Formation of the dinitrobenzene–glutathione conjugate via nucleophilic displacement of fluor with GSH-thiol was monitored spectrophotometrically at 340 nm for 5.0 min (kinetic mode, three scans/min) on an Eppendorf spectrophotometer; time–response curves were built. Dinitrobenzene–glutathione conjugate concentration was calculated via an extinction coefficient of 9.6 mM^{-1} cm^{-1} (Mazari et al., 2015). The lysate preparations and worm incubation medium samples were assayed in triplicate. Control reactions (without the enzyme) were included to determine non-enzymatic conjugation. Ethacrynic acid (EA; 6–200 μM) served as an inhibitor of GST σ. The concentration-dependent inhibitory activity of RSV and EA were derived from the set of time–response curves (combined data from lysate and medium). Four parameter logistic regression was used to calculate the half-maximal effective dose (ED_{50}) and standard error values for RSV and EA ('drc' R 3.6.0 package, $P < 0.05$).

2.10. In vitro chemotherapy

Adult worms were recovered from the livers of untreated hamsters, pooled and thoroughly washed with sterile saline (0.9% NaCl). The worms were incubated at 37 °C for 24 h (Mordvinov et al., 2017; Pakharukova et al., 2018, 2019b). Praziquantel (Sigma–Aldrich, USA) and RSV were dissolved in dimethyl sulfoxide (DMSO) (Sigma–Aldrich) to obtain 1 mM stock solutions. For calculation of the half-maximal inhibitory concentration (IC_{50}), we tested the following concentrations of compounds: 0.01, 0.1, 1, 10, 100, and 500 μM. Four to five adult worms per well of a 12-well culture plate were analysed. The solvent (DMSO) concen-

tration across different compound concentrations was 0.5% v/v. As control groups, we used flukes incubated in the medium with 0.5% DMSO. The experiments were repeated three times. Next, after 24 h of treatment with one of the drugs, viability of the worms was evaluated under an inverted microscope (Axiovert 40CFL) equipped with a camera (Axiocam ICC3, Zeiss) (magnification 10–50×). The motility of viable worms was assessed by motility tests (Mordvinov et al., 2017; Pakharukova et al., 2018, 2019b). The IC_{50} and IC_{95} values, defined as the concentration of a drug required to the decrease the mean worm's motility to 50% and 95% at the 24 h time point, was expressed using CompuSyn software (version 1.0) (Chou, 2010).

2.11. Statistics

The data were subjected to statistical analysis in the Statistica 6.0 software (Statsoft, USA). The *F*-test with the Newman–Keuls post hoc analysis was applied to significant main effects and interactions to assess the differences in some means (western blot, RT-PCR data and 8OH-dG levels).

Significance of the differences between the groups of hamsters was evaluated by the Mann–Whitney test (cut-off $P < 0.05$) in Statistica 6.0 (histopathology and serum biochemical data). The dose–effect relation of RSV in GST σ activity measurements was assessed by linear regression analysis.

3. Results

3.1. Opisthorchis felineus GST-σ was found in the epithelium of bile ducts of experimental animals

Using specific antiserum against *O. felineus* GST σ, we found that this parasitic protein was present in the cells of the bile ducts of infected animals at 1 (Fig. 1) and 3 months p.i. (data not shown), whereas no immunoreactivity with the antibodies was observed in the cells of the bile ducts of uninfected animals. Thus, the parasitic protein was secreted into bile ducts and persisted in the epithelium of bile ducts.

3.2. Activity of O. felineus GST σ

To evaluate the enzymatic activity of *O. felineus* GST σ, the worm incubation medium and the worm lysates were analysed, extracted from animals at 1 month and 3 months p.i. EA was chosen as an inhibitor. Enzymatic activity was detected both in the helminth lysates and in the worm incubation medium (Supplementary Table S3). RSV was found to suppress the enzymatic activity in a dose-dependent manner (linear regression: $R = 0.85$, degrees of freedom [*df*] = 1, $F = 33.02$, $P = 0.00009$, Supplementary Table S3). The ED_{50} values for RSV and ethacrynic acid were quite similar: 48.6 ± 5.4 and 32.9 ± 3.1 μM, respectively (Fig. 2).

Because parasitic GST σ was found in the bile ducts of the experimental hamsters, this enzyme might contribute to the pathogenesis of opisthorchiasis. Accordingly, we decided to evaluate the influence of parasitic enzyme inhibitor RSV on the progression of precancerous lesions and the expression of neoplasia markers in the experimental opisthorchiasis.

3.3. Liver histopathology

Bile ducts of the liver from the hamsters infected for 1 and 3 months (Fig. 3) were found to be lined by an epithelium with enlarged nuclei, showing a loss of polarity and mitotic figures (Fig. 3C and E). Cholangiocyte atypia was noticed. A transition from the normal duct epithelium (Fig. 3A and B) to an atypical lesion was observed (Fig. 3C and E). According to the conclusions of the international interobserver agreement study on the diagnosis of biliary epithelium dysplasia (Zen et al., 2007), biliary intraepithelial neoplasia (BilIN) is classified into three categories based on the degree of atypia: BilIN-1, BilIN-2, and BilIN-3, which reflect a multistep sequence with an increasing neoplastic potential (Zen et al., 2007). We noted BilIN-1 at 1 month p.i. and BilIN-2 at 3 months p.i. (Fig. 3C and E).

Granulomatous inflammation and mononuclear cell and eosinophilic infiltration of the portal area in the periductal tissue and in liver parenchyma were also evident (Fig. 3C–E). Additionally, in the duct lumens of the hamsters infected for 3 months, we detected polyps that were infiltrated by inflammatory cells, the

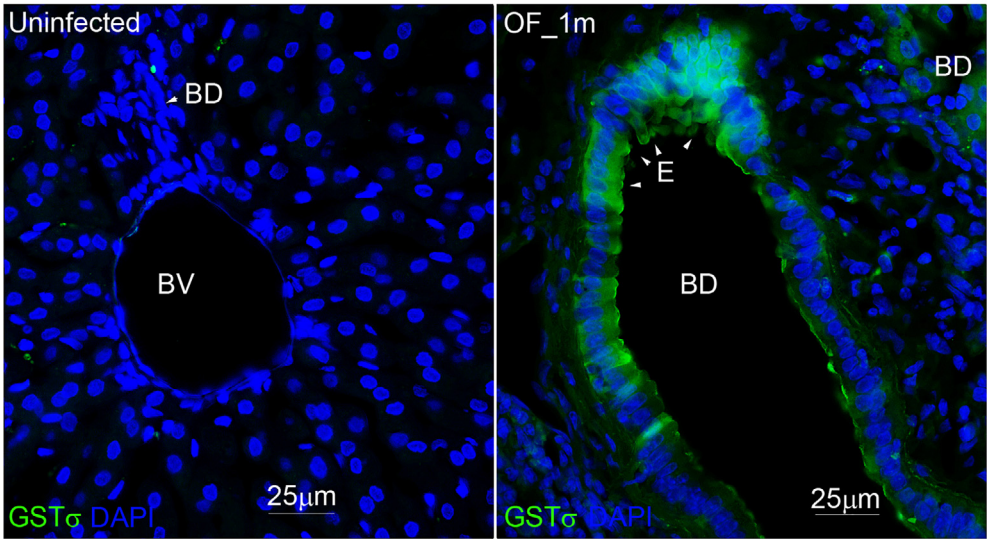

Fig. 1. Parasitic glutathione-dependent prostaglandin synthase (GST σ) in the epithelium of bile ducts in infected hamsters. Cell nuclei are stained blue by DAPI, GST σ is stained with the antiserum against recombinant *Opisthorchis felineus* GST σ. BD, bile duct; BV, blood vessel; E, epithelial cells of the bile duct; OF_1m: 1 month p.i. with *O. felineus*.

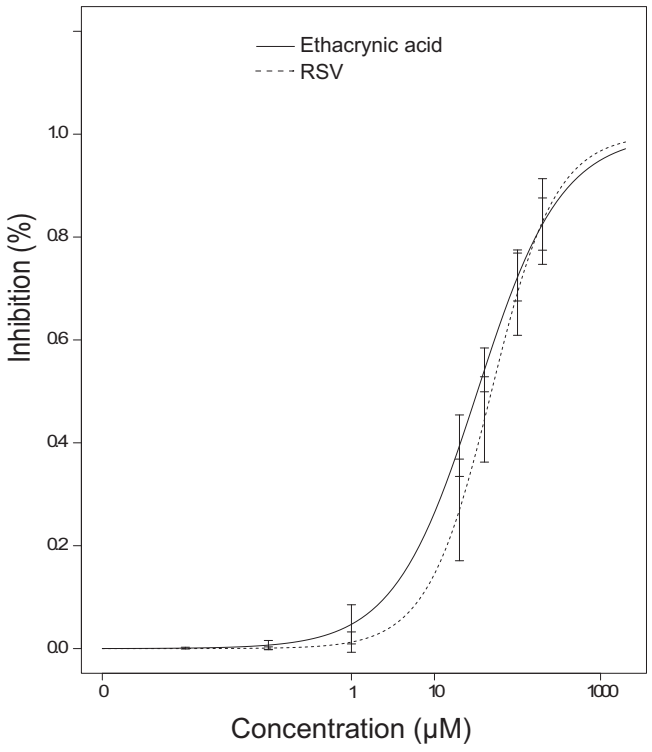

Fig. 2. The concentration-dependent inhibitory activity of resveratrol (RSV) and ethacrynic acid (EA). The data were derived from a set of time–response curves constructed for dinitrobenzene–glutathione conjugation as described elsewhere (Mazari et al., 2015). Four-parameter logistic regression was used to calculate the half-maximal effective dose (ED_{50}) and standard error values for RSV and EA ('drc' R 3.6.0 package), $P < 0.05$.

parasite's eggs, and a dark pigment (egg granuloma was not noted). The major histological changes observed in the gallbladder and extrahepatic bile ducts comprised epithelial hyperplasia and chronic inflammation (Fig. 3C and E). Van Gieson's stain uncovered massive periportal fibrosis (Supplementary Fig. S1).

The liver histopathology in the infected hamsters treated with RSV also showed the signs of epithelial hyperplasia, periductal fibrosis, and chronic inflammation (Fig. 3D and F, Supplementary Fig. S1(A–F)). Nonetheless, the degree of histopathological lesions in the liver was lower, in particular, quantitative analysis of these parameters detected a significant reduction in mononuclear cell and eosinophilic infiltration (a twofold decrease at 3 months p.i.: $P = 0.005$, $n = 7$, Supplementary Table S1; Fig. 4A) in the periductal and liver parenchyma as well as egg granuloma (a twofold decrease at 3 months p.i.: $P = 0.04$, $n = 7$, Supplementary Table S1; Fig. 4A). Hyperplasia of cholangiocytes was also attenuated (a 2.2-fold decrease at 1 month p.i.: $P = 0.04$, $n = 5$; a 1.5-fold decrease at 3 months p.i.: $P = 0.009$, $n = 7$, Supplementary Table S1). One of the conspicuous results was significant downregulation of biliary intraepithelial neoplasia (a 1.8-fold decrease, $P = 0.008$, $n = 7$, Supplementary Table S1; Fig. 4A) and metaplasia (a 10-fold decrease, $P = 0.008$, $n = 7$, Supplementary Table S1; Fig. 4A).

It was reported that infection with liver flukes can induce oxidative DNA damage (Yongvanit et al., 2012). This observation prompted us to test whether experimental opisthorchiasis leads to 8-hydroxy-2′-deoxyguanosine (8OH-dG) formation. Indeed, the level of 8OH-dG in urine increased in the hamsters with opisthorchiasis at 1 month p.i. (a 6.7-fold increase; $P = 0.0015$) and at 3 months p.i. (a 3.2-fold increase; $P = 0.039$; Fig. 4B). RSV significantly attenuated the elevation of 8OH-dG concentration at 3 months p.i. (a 3.8-fold decrease; $P = 0.04$; Fig. 4B).

3.4. In vitro chemotherapy

To demonstrate that reduction of inflammation and neoplasia by RSV was not caused by its anthelmintic effect, we tested its anthelmintic activity in vitro on adult worms. Testing revealed that the anthelmintic activity of RSV ($IC_{50} = 259$ μM; $IC_{95} = 2890$ μM) was almost negligible, in particular 500-fold weaker than that of praziquantel ($IC_{50} = 0.47$ μM; $IC_{95} = 2.64$ μM). Thus, it is unlikely that resveratrol could have a significant anthelmintic effect in vivo in the absence of it occurring in vitro.

3.5. Expression of the genes involved in hyperplasia and fibrogenesis

3.5.1. mRNA expression

The relative expression levels of cytokeratin 7 (*Ck7* as a marker of cholangiocyte hyperplasia were low in the uninfected animals. There was strong upregulation of *Ck7* mRNA at 1 month p.i. ($P = 0.01$, a 17-fold increase) and 3 months p.i. ($P = 0.01$, a 19-fold increase, Fig. 5A), which was consistent with the data on hyperplasia obtained from liver histopathology (Fig. 4A). To evaluate fibrogenesis, we evaluated the expression levels of smooth muscle actin alpha (α-SMA, *Acta2* gene) and transforming growth factor beta (*Tgfb*). In the uninfected groups, *Acta2* and *Tgfb* expression was low (Fig. 5B and C). The greatest *Acta2* expression was observed in the *O. felineus*–infected groups at 1 month p.i. (a six-fold increase; $P = 0.008$) and 3 months p.i. (a 16-fold increase; $P = 0.03$). The elevated *Tgfb* expression was also demonstrated in *O. felineus*–infected groups at 1 and 3 months p.i. (a 2.8- and four-fold increase, respectively; Fig. 5C).

RSV significantly attenuated the *Ck7* mRNA upregulation as a marker of cholangiocyte hyperplasia (an 8.5- and 4-fold decrease, respectively). Moreover, RSV decreased the elevated mRNA expression of *Acta2* (a 2.9-fold decrease, $P = 0.009$ at 1 month p.i.; a 16-fold decrease, $P = 0.037$ at 3 months p.i.; Fig. 5B). The influence of RSV on *Tgfb* expression was non-significant (Fig. 5C).

3.5.2. Protein expression

To assess fibrogenesis at the protein expression level, we measured the protein level of α-SMA (Fig. 6A and B). The highest α-SMA content was observed in the *O. felineus*–infected groups at 1 month p.i. ($P = 0.0008$) and 3 months p.i. ($P = 0.006$) as depicted in Fig. 6B.

A high protein level was also demonstrated for cholangiocyte hyperplasia marker CK7 in the liver of *O. felineus*-infected animals, in line with the data on the mRNA expression of this gene. The CK7 protein amount increased in a time-dependent manner (5- and 14-fold higher at 1 and 3 months p.i., respectively). These data were in agreement with liver histopathology findings showing substantial hyperplasia (Fig. 4A, Supplementary Table S1). In addition to that, proliferating cell nuclear antigen (PCNA) content was also significantly higher in *O. felineus*-infected animals (7- and 15-fold higher at 1 and 3 months p.i., respectively, Fig. 6D) compared with the uninfected ones, which apparently indicates there are active proliferative processes in the tissue. A change in the expression of E-cadherin as the prototypical epithelial cell marker plays a key role in cellular adhesion; the loss of this function has been associated with tumour metastasis (Padthaisong et al., 2017). Nevertheless, no significant differences in the amount of E-cadherin were detected (Fig. 6A and E).

In agreement with the results on mRNA expression, RSV significantly decreased elevated amounts of the α-SMA protein at 1 month p.i. (a 1.5-fold decrease; $P = 0.045$) and 3 months p.i. (a 2.9-fold decrease; $P = 0.045$; Fig. 6A and B). RSV attenuated the upregulation of CK7 (a 2.9-fold decrease; $P = 0.0001$) and PCNA (a 2.1-fold decrease; $P = 0.002$) in *O. felineus*–infected animals (Fig. 6A, C, and D) at 3 months p.i.

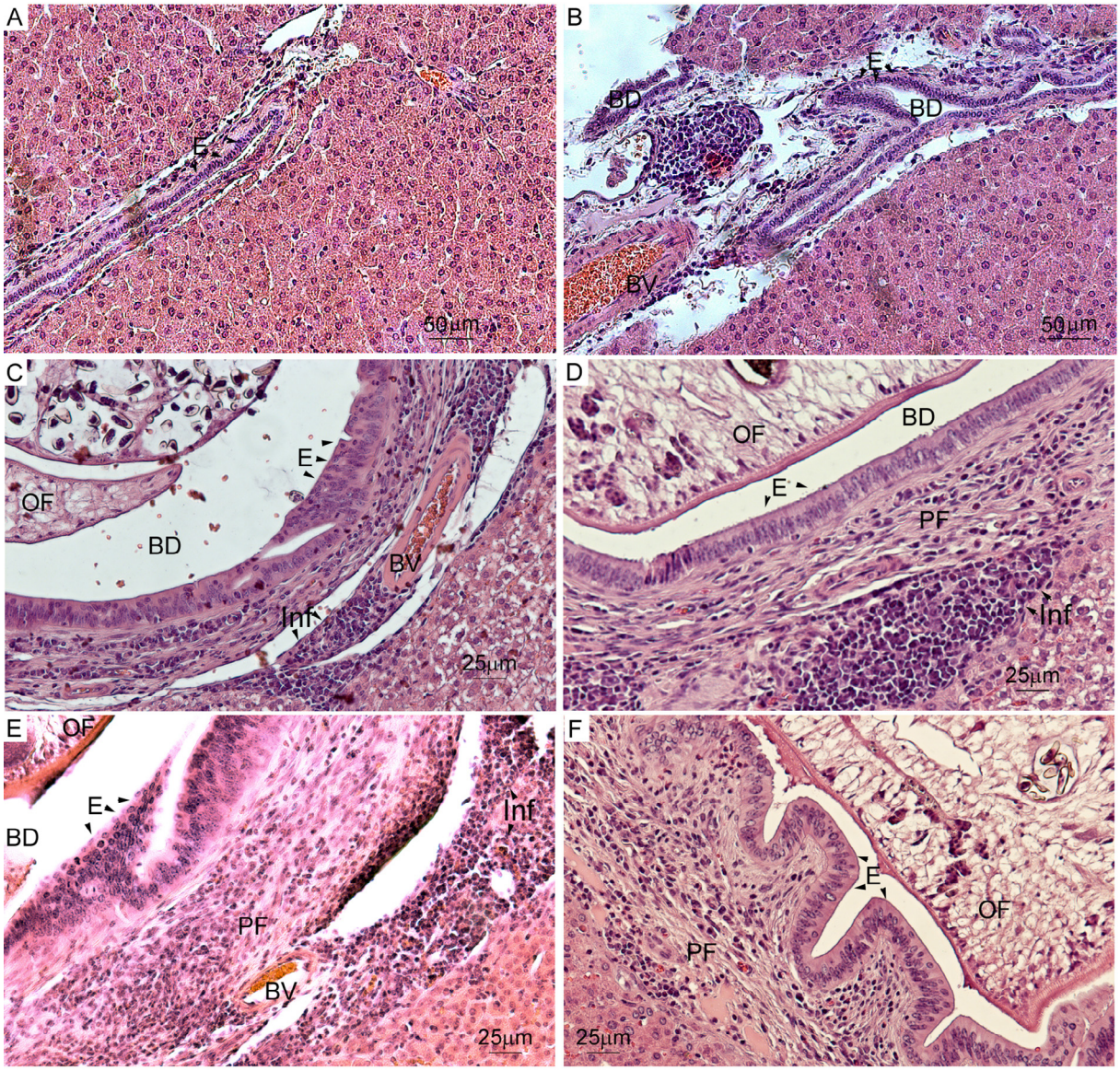

Fig. 3. Biliary histological features observed in the liver biopsies from uninfected and infected hamsters (H&E staining). (A) Uninfected; (B) Resveratrol (RSV) at 1 month p.i.; (C) *Opisthorchis felineus* (OF)-infected; (D) OF + RSV at 1 month p.i.; (E) OF-infected at 3 months p.i.; (F) OF + RSV at 3 months p.i. BD, bile duct; PF, periductal fibrosis; BV, blood vessel; E, epithelial cells of bile duct; Inf, inflammatory cell infiltration.

3.6. Serum biochemistry

More than twofold increases in ALT and AST activities are usually used to detect liver damage and/or to help diagnose liver dysfunction (Bakshtanovskaia and Stepanova, 2005). The activity of ALT in the infected animals increased dramatically at 1 and 3 months p.i. (6.8- and 10-fold elevation, respectively, Fig. 7A; Supplementary Table S4). At this time point, RSV significantly downregulated ALT (a 1.6-fold decrease at 3 months p.i.; Mann–Whitney test: $U = 0$, $P = 0.004$; Fig. 7A; Supplementary Table S4), but the level was still 6-fold higher compared with uninfected animals. RSV did not significantly change ALT at 1 month p.i. At 1 month p.i., AST activity showed a tendency to increase, and at 3 months p.i., AST activity was twofold higher (Mann–Whitney test: $U = 0$, $P = 0.02$) in the infected hamsters than in the uninfected hamsters (Fig. 7B; Supplementary Table S4). RSV significantly reduced AST activity in the infected animals at 3 months p.i. (a 1.6-fold decrease; Mann–Whitney test: $U = 0$, $P = 0.02$; Fig. 7B; Supplementary Table S4).

Abnormalities of cholesterol metabolism and pronounced upregulation of serum bilirubin are associated with cholestasis and biliary injury (Longo et al., 2001). These increases in the levels of bilirubin, ALT, and cholesterol are registered in patients with chronic opisthorchiasis (Bakshtanovskaia and Stepanova, 2005). We showed that bilirubin was significantly upregulated at 1 and 3 months p.i. compared with uninfected animals (3.4-fold and 3-fold, respectively; Fig. 7C; Supplementary Table S4). The cholesterol level was also elevated at 1 and 3 months p.i. (a 1.8- and 1.8-fold increase, respectively, Fig. 7D; Supplementary Table S4). RSV significantly reduced the level of bilirubin at 1 month p.i. (a twofold decrease; Mann–Whitney test: $U = 0$, $P = 0.02$; Fig. 7C; Supplementary Table S4), attenuated the increase in the choles-

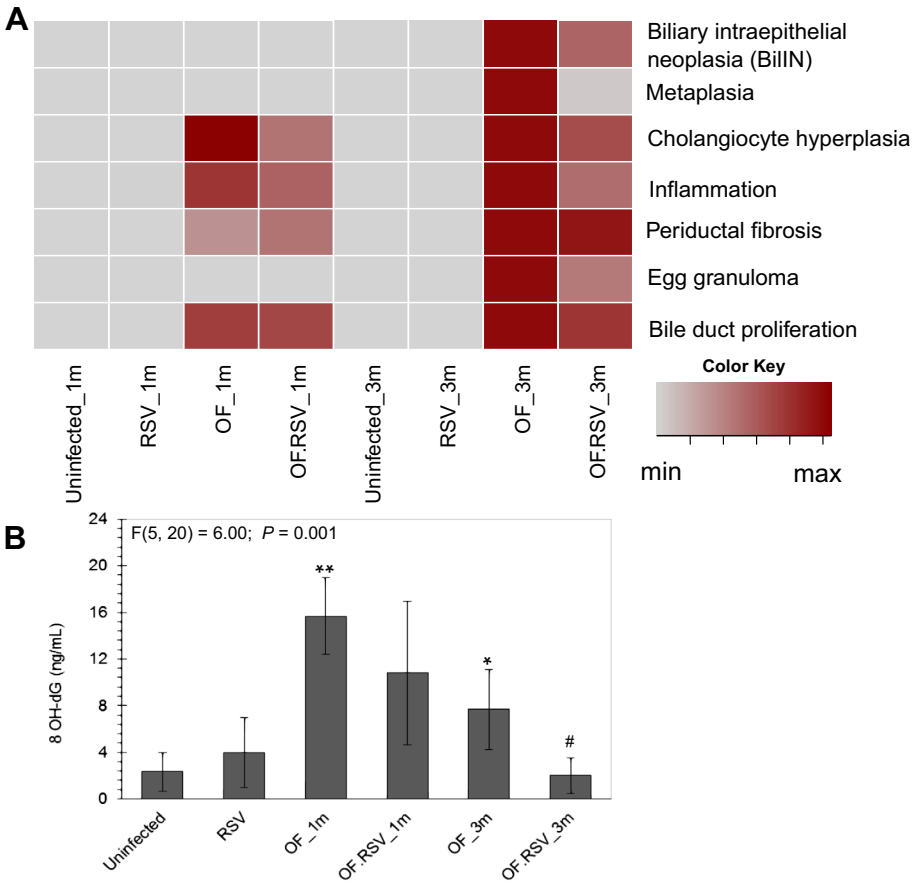

Fig. 4. Inflammation, cholangiocyte hyperplasia, bile duct dysplasia, and oxidative DNA lesions in the liver of hamsters with opisthorchiasis felinea (at 1 and 3 months (m) p.i. with *Opisthorchis felineus* (OF)). (A) Liver histopathology analysis. Each field of view (20–30 fields) was divided into 100 squares in Morphometry software. Histopathological changes were assessed by means of a percentage of the area (the number of squares occupied). The data are expressed as a percentage of the maximal possible score and presented as a heat map using the heatmap.2 (v.2.38) R package. Detailed data are presented in Supplementary Table S1. (B) Urinary 8-hydroxy-2′-deoxyguanosine (8OH-dG) levels in hamsters with opisthorchiasis. The data are shown as mean ± S.D. $^{*\#}P < 0.05$; $^{**}P < 0.01$ (*compared with the uninfected group, # compared to the OF_3m group).

terol level (a 1.5-fold decrease; Mann–Whitney test: $U = 0$, $P = 0.033$; Fig. 7D) at 3 months p.i, and did not significantly change the cholesterol level at 1 month p.i.

4. Discussion

Opishthorchis felineus–associated chronic inflammation increases oxidative stress, which can overwhelm antioxidant system homeostasis to dampen reactive oxygen species production and consequent oxidative modification of host biomolecules, including DNA (Gouveia et al., 2017; Pakharukova et al., 2019c). The chronic inflammation facilitates myofibroblast activation, high-grade cholangiocyte neoplasia, and periductal fibrosis (Maksimova et al., 2017; Yazdani et al., 2017). Myofibroblasts (the key players in extracellular matrix remodelling) are characterised by α-SMA expression and an ability to secrete a wide range of mediators including TGF-β, cytokines, growth factors, proinflammatory chemokines, and other factors, which either directly affect tissues (extracellular matrix remodelling) or act on other cells in a paracrine fashion (Yazdani et al., 2017). This action has a number of effects such as epithelial cell activation and dedifferentiation (high-grade biliary neoplasia), immune activation, fibrosis, and elevated *Tgfb*, *α-SMA*, *CK7*, and *PCNA* expression.

Chronic inflammation associated with liver fluke infection might be provoked and exacerbated by (i) the mechanical damage to cells by the flukes, (ii) the reactive oxygen species generated by host cells at the site of inflammation, and (iii) the effects of proteins and metabolites secreted by liver flukes (Chaiyadet et al., 2015; Gouveia et al., 2017; Petrenko et al., 2017). Excretory–secretory product proteins can interact with the epithelium and accumulate inside the cells (Fig. 1). Other damaging agents that can contribute to chronic inflammation are parasitic oxysterol-like metabolites (Correia da Costa et al., 2014; Gouveia et al., 2017), which possess genotoxic and pro-oxidative properties (Cavalieri and Rogan, 2010). Oxysterols might be generated by a non-enzymatic reaction with oxidative free radical-like oxygen and nitrogen species. They could also originate as products of enzymatic activity of the parasites (Pakharukova et al., 2012, 2015). Associations between oxysterols and the initiation and progression of colon, lung, breast, and bile duct cancers have been suggested (Jaworski et al., 2001; Cavalieri and Rogan, 2010; Kuver, 2012; Correia da Costa et al., 2014). These processes cause damage to the genetic material, malignant transformation of cells, and CCA progression (Sripa et al., 2012, 2018; Yongvanit et al., 2012; Chaiyadet et al., 2015).

To understand the mechanisms that underlie precancerous lesion formation in the liver, in particular high-grade epithelial

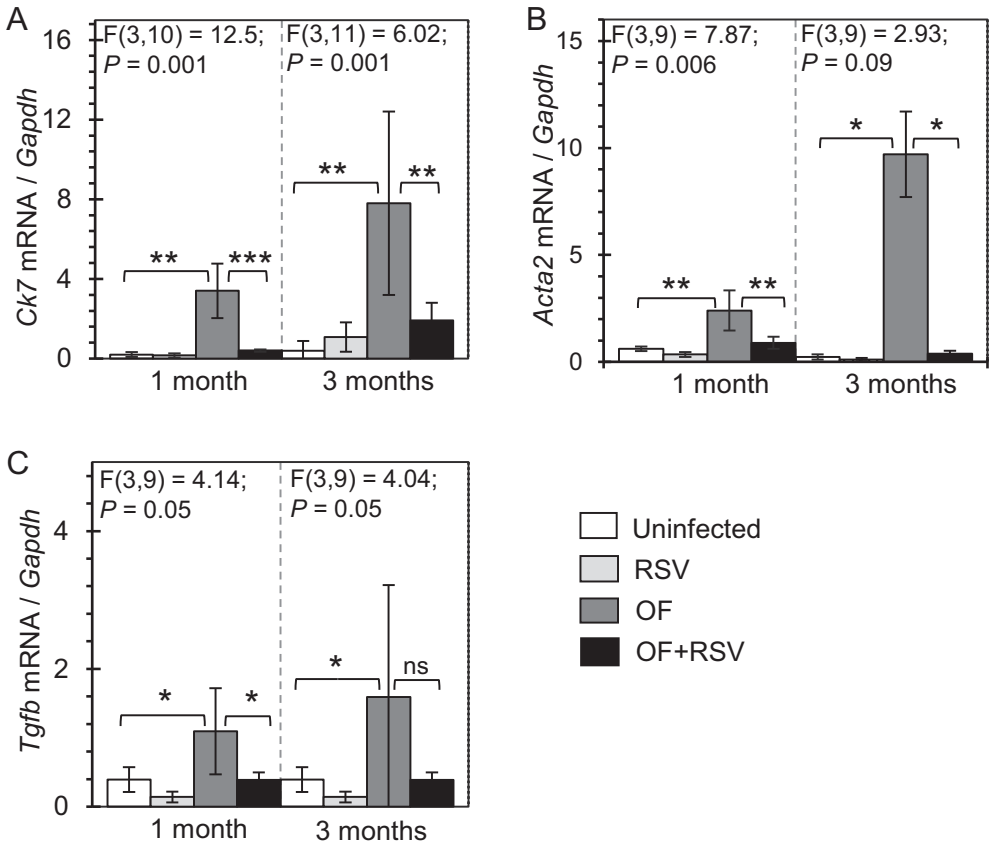

Fig. 5. mRNA expression of the genes involved in hyperplasia and fibrogenesis. Data are presented as a fold-change in mRNA expression normalised to *Gapdh* mRNA expression and are expressed as mean ± S.D. OF, *Opisthorchis felineus*-infected; RSV, resveratrol; *Acta2*, smooth muscle actin α; *Ck7*, cytokeratin 7; *Tgfb*, transforming growth factor β; ns, non-significant. $^{*}P < 0.05$; $^{**}P < 0.01$; $^{***}P < 0.001$.

neoplasia, we investigated the impact of RSV as a natural antioxidant and an inhibitor of an extracellular parasitic prostaglandin synthase on the progression of epithelial neoplasia and the functional state of the liver in acute and chronic opisthorchiasis. An additional factor in favour of the choice of RSV was its ability to reduce the formation of oxysterols and oestrogen–DNA adducts (Cavalieri and Rogan, 2010).

Extracellular parasitic GST σ may participate in the modulation of host immunity by contributing to the production of prostanoids, as demonstrated for the extracellular GST1 from *O. volvulus* (Sommer et al., 2003). The physiological importance of prostanoid synthesis by *O. felineus* GST-σ for the pathogenesis of liver fluke infection is not clear. Nevertheless, because prostaglandins contribute to the induction and progression of excessive and chronic inflammatory responses, it is possible that the inhibitory action of RSV on parasitic excretory prostaglandin synthase contributed to its anti-inflammatory effect and to the attenuation of cholangiocyte neoplasia.

We demonstrated significant alleviation of high-grade neoplasia of cholangiocytes in the experimental model of opisthorchiasis felinea. Reductions in the mRNA and protein expression of *Ck7* after RSV treatment support the histopathological findings. Additionally, downregulation of PCNA indicates inhibition of cell proliferation in the liver of the hamsters.

Furthermore, another explanation of the neoplasia suppression by RSV might be the inhibition of cell signalling pathways. RSV is a natural activator of *Sirt1*. Protein deacetylase SIRT1 (Fourcade et al., 2015; Xiao et al., 2016) participates in many cellular processes such as cell cycle regulation and a cellular stress response (Xiao et al., 2016) by activating or deactivating transcription factors and regulatory proteins (Widlund et al., 2013; Fourcade et al., 2015). In particular, RSV can inhibit tissue injury and chronic inflammation via inactivation of the TGF-β pathway and the interaction of proteins in the mTOR cascade, thus suppressing mTOR mitogenic signalling (Widlund et al., 2013). Furthermore, RSV might reduce inflammation by inhibiting the phosphorylation and nuclear translocation of NF-κB p65, thereby suppressing the NF-κB signalling pathway (Kang et al., 2018).

Another way to alleviate inflammation might be to reverse mitochondrial dysfunction, which might be caused by a chronic redox imbalance and oxidative lesions (Fourcade et al., 2015). Via SIRT1, RSV activates mitochondrial biogenesis by activating PGC-1 and thus normalises mitochondrial content and redox homeostasis, and alleviates inflammation (Fourcade et al., 2015).

Which pathway is suppressed by RSV in chronic opisthorchiasis and underlies the neoplasia suppression by RSV is the subject of future research. Our present data provide first insights into the mechanism by which *O. felineus* infection causes liver injuries, and we present the results on myofibroblast activation and the expression of hyperplasia- and fibrogenesis-related proteins. RSV inhibited the extracellular parasitic GST-σ and reduced epithelial neoplasia and oxidative DNA lesions. The objective of this project was to explore new research ideas, and all our hypotheses require further investigation and experimental validation. RSV can

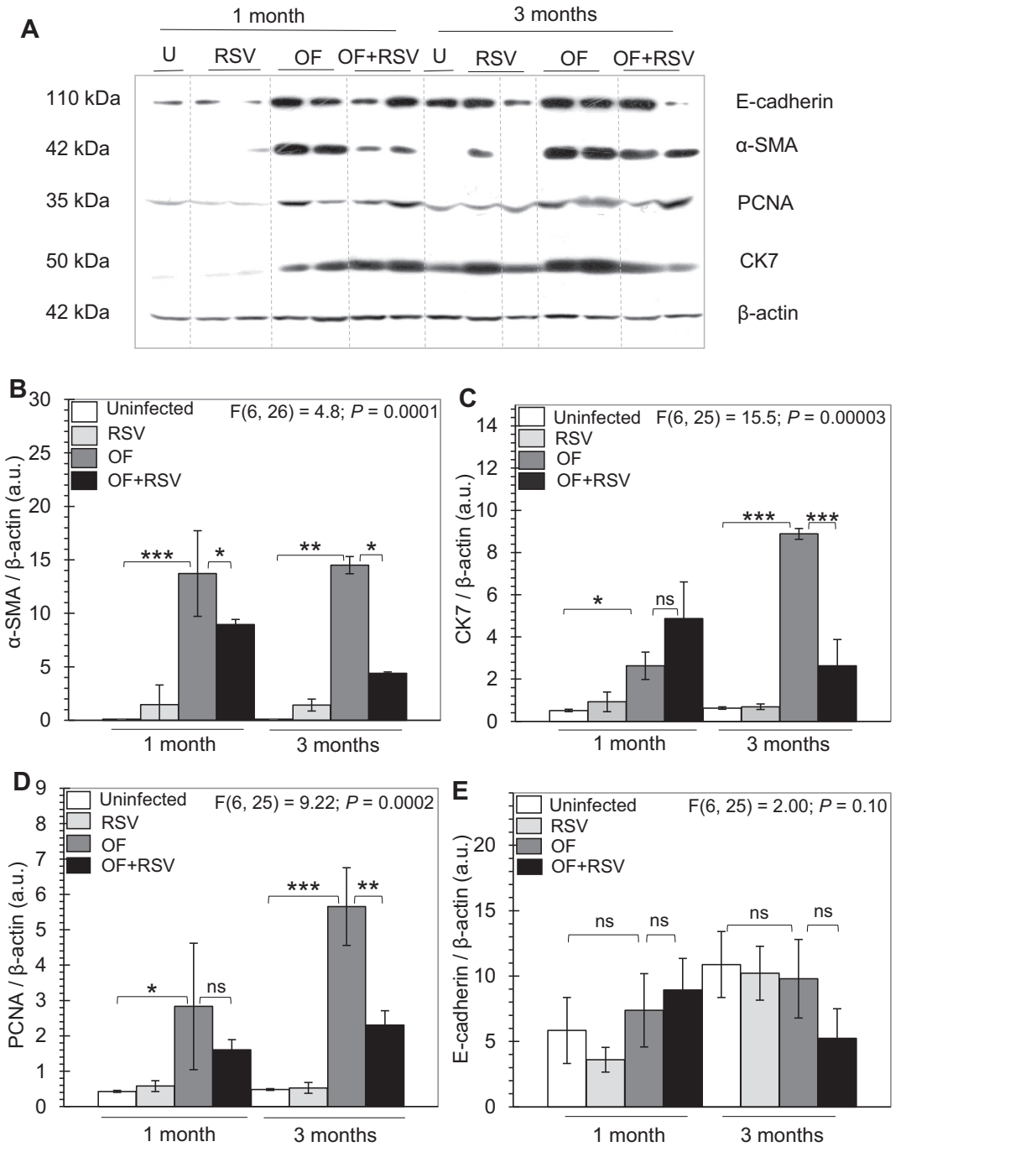

Fig. 6. Elevated levels of cell proliferation, fibrosis, and neoplasia markers in hamsters, uninfected or infected with *Opisthorchis felineus*. (A) Western blotting of protein markers E-cadherin, smooth muscle actin α (α-SMA), proliferating cell nuclear antigen (PCNA), and CK7 (cytokeratin 7; with a β-actin loading control), which are quantified in subsequent panels. Representative immunoblots are shown. Immunoblotting was performed three times. U, uninfected; OF, *O. felineus*–infected; RSV, resveratrol, (B–E) Densitometry results (quantified cell marker intensity relative to the β-actin loading control). (B) α-SMA, (C) CK7, (D) PCNA, (E) E-cadherin. The data are expressed as mean ± S.D. $^{*}P < 0.05$, $^{**}P < 0.01$, $^{***}P < 0.001$. ns, non-significant.

influence a wide range of pathways; therefore, the supposition that RSV helps to reduce damage only via GST σ inhibition is a big assumption. Future experiments are needed to confirm the role of GST σ in *O. felineus* pathogenicity, e.g., RNA interference or CRISPR/Cas9 knockout experiments for reducing the expression of GST σ, as was clearly demonstrated for *O. viverrini* granulin 1 (Arunsan et al., 2019). The results of CRISPR/Cas9 genome editing of *O. viverrini* granulin-1 proved the hypothesis about its involvement in the hepatobiliary morbidity of liver fluke infection (Arunsan et al., 2019).

Although the specific mechanisms of action of RSV remain unclear, our results from the hamster model represent a compelling argument for the testing of RSV in combination chemotherapy of opisthorchiasis. The chemopreventive effect of RSV targeting GST σ activity might be useful for improving the outcomes in infected populations and for prevention of the infection-related CCA.

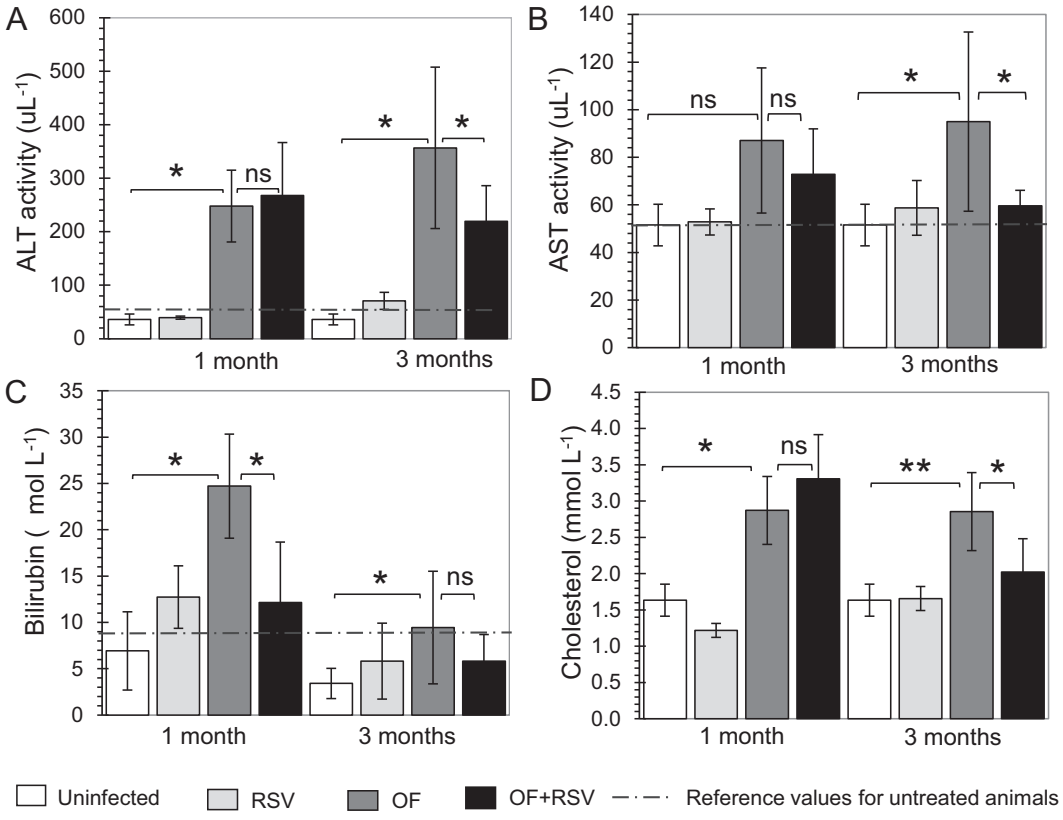

Fig. 7. Serum parameters in hamsters, uninfected or infected with *Opisthorchis felineus* at 1 and 3 months p.i.. (A) aspartate aminotransferase (AST); (B) cholesterol; (C) alanine transaminase (ALT); (D) bilirubin. The data are shown as mean ± S.D. *P* values were calculated by the Mann–Whitney *U* test, $^{*}P < 0.05$; $^{**}P < 0.01$. Reference values for untreated animals (Van Hoosier and McPherson, 1987; Field and Sibold, 1998) are indicated as horizontal dashed lines. The details are presented in Supplementary Table S4. OF, *O. felineus*–infected; RSV, resveratrol.

Acknowledgements

The authors are grateful to Mikhail Pomaznoy from the Institute of Cytology and Genetics, Siberian Branch of the Russian Academy of Sciences, Russia (ICG SB RAS) for the antiserum against recombinant O. felineus GST σ. Microscopy was performed at the Microscopy Center of the ICG SB RAS. The authors acknowledge the support and collaboration of members of the Tomsk Opisthorchiasis Consortium (TOPIC). This work was supported financially by the Russian Science Foundation (grant number 18-15-00098 (VAM)). The funding agency had no role in this study, e.g., in study design, data collection, or decision to publish.

Appendix A. Supplementary data

Supplementary data to this article can be found online at https://doi.org/10.1016/j.ijpara.2019.07.002.

References

Armignacco, O., Ferri, F., Gomez-Morales, M.A., Caterini, L., Pozio, E., 2013. Cryptic and asymptomatic *Opisthorchis felineus* infections. Am. J. Trop. Med. Hyg. 88, 364–366.

Arunsan, P., Ittiprasert, W., Smout, M.J., Cochran, C.J., Mann, V.H., Chaiyadet, S., Karinshak, S.E., Sripa, B., Young, N.D., Sotillo, J., Loukas, A., Brindley, P.J., Laha, T., 2019. Programmed knockout mutation of liver fluke granulin attenuates virulence of infection-induced hepatobiliary morbidity. Elife 15 (8), pii: e41463.

Bakshtanovskaia, I.B., Stepanova, T.F., 2005. Analysis of a complex of biochemical parameters of hepatic functions in opisthorchiasis. Med. Parazitol. Parazit. Bol. 4, 18–21.

Baur, J.A., Sinclair, D.A., 2006. Therapeutic potential of resveratrol: the *in vivo* evidence. Nat Rev. Drug. Discov. 5, 493–506.

Cavalieri, E.L., Rogan, E.G., 2010. Depurinating estrogen-DNA adducts in the etiology and prevention of breast and other human cancers. Future Oncol. 6, 75–91.

Chaiyadet, S., Sotillo, J., Smout, M., Cantacessi, C., Jones, M.K., Johnson, M.S., Turnbull, L., Whitchurch, C.B., Potriquet, J., Laohaviroj, M., Mulvenna, J., Brindley, P.J., Bethony, J.M., Laha, T., Sripa, B., Loukas, A., 2015. Carcinogenic liver fluke secretes extracellular vesicles that promote cholangiocytes to adopt a tumorigenic phenotype. J. Infect. Dis. 212, 1636–1645.

Chou, T.C., 2010. Drug combination studies and their synergy quantification using the Chou-Talalay method. Cancer Res. 70, 440–446.

Correia da Costa, J.M., Vale, N., Gouveia, M.J., Botelho, M.C., Sripa, B., Santos, L.L., Santos, J.H., Rinaldi, G., Brindley, P.J., 2014. Schistosome and liver fluke derived catechol-estrogens and helminth associated cancer. Front. Genet. 5, 444–447.

Ershov, N.I., Mordvinov, V.A., Prokhortchouk, E.B., Pakharukova, M.Y., Gunbin, K.V., Ustyantsev, K., Genaev, M.A., Blinov, A.G., Mazur, A., Boulygina, E., Tsygankova, S., Khrameeva, E., Chekanov, N., Fan, G., Xiao, A., Zhang, H., Xu, X., Yang, H., Solovyev, V., Lee, S.M., Liu, X., Afonnikov, D.A., Skryabin, K.G., 2019. New insights from *Opisthorchis felineus* genome: update on genomics of the epidemiologically important liver flukes. BMC Genomics 20 (1), 399.

Field, K.J., Sibold, A.L., 1998. The Laboratory Hamster and Gerbil. CRC Press, New York.

Fourcade, S., Ferrer, I., Pujol, A., 2015. Oxidative stress, mitochondrial and proteostasis malfunction in adrenoleukodystrophy: a paradigm for axonal degeneration. Free Radic. Biol. Med. 88 (Pt A), 18–29.

Gibson-Corley, K.N., Olivier, A.K., Meyerholz, D.K., 2013. Principles for valid histopathologic scoring in research. Vet. Pathol. 50, 1007–1015.

Girbovan, C., Plamondon, H., 2015. Resveratrol downregulates type-1 glutamate transporter expression and microglia activation in the hippocampus following cerebral ischemia reperfusion in rats. Brain Res. 1608, 203–214.

Gouveia, M.J., Pakharukova, M.Y., Laha, T., Sripa, B., Maksimova, G.A., Rinaldi, G., Brindley, P.J., Mordvinov, V.A., Amaro, T., Santos, L.L., Costa, J.M.C.D., Vale, N., 2017. Infection with *Opisthorchis felineus* induces intraepithelial neoplasia of the biliary tract in a rodent model. Carcinogenesis 38, 929–937.

Jang, M., Cai, L., Udeani, G.O., Slowing, K.V., Thomas, C.F., Beecher, C.W., Fong, H.H., Farnsworth, N.R., Kinghorn, A.D., Mehta, R.G., Moon, R.C., Pezzuto, J.M., 1997. Cancer chemopreventive activity of resveratrol, a natural product derived from grapes. Science 275, 218–220.

Jaworski, C.J., Moreira, E., Li, A., Lee, R., Rodriguez, I.R., 2001. A family of 12 human gene containing oxysterol-binding domains. Genomics 78, 185–196.
Kang, D.G., Lee, H.J., Lee, C.J., Park, J.S., 2018. Inhibition of the expression of matrix metalloproteinases in articular chondrocytes by resveratrol through affecting nuclear factor-kappa B signaling pathway. Biomol. Ther. (Seoul) 26, 560–567.
Klopfleisch, R., 2013. Multiparametric and semiquantitative scoring systems for the evaluation of mouse model histopathology-a systematic review. BMC Vet. Res. 9, 123.
Kuver, R., 2012. Mechanisms of oxysterol-induced disease: insight from the biliary system. Clin. Lipidol. 7, 537–548.
Longo, M., Crosignani, A., Podda, M., 2001. Hyperlipidemia in chronic cholestatic liver disease. Curr. Treat. Options Gastroenterol. 4, 111–114.
Lvova, M.N., Duzhak, T.G., Tsentalovich, Iu.P., Katokhin, A.V., Mordvinov, V.A., 2014. Secretome of the adult liver fluke *Opisthorchis felineus*. Parazitologiia 48, 169–184.
Maksimova, G.A., Pakharukova, M.Y., Kashina, E.V., Zhukova, N.A., Kovner, A.V., Lvova, M.N., Katokhin, A.V., Tolstikova, T.G., Sripa, B., Mordvinov, V.A., 2017. Effect of *Opisthorchis felineus* infection and dimethylnitrosamine administration on the induction of cholangiocarcinoma in Syrian hamsters. Parasitol. Int. 66, 458–463.
Mazari, A.M., Hegazy, U.M., Mannervik, B., 2015. Identification of new inhibitors for human hematopoietic prostaglandin D2 synthase among FDA-approved drugs and other compounds. Chem. Biol. Interact. 229, 91–99.
Mordvinov, V.A., Shilov, A.G., Pakharukova, M.Y., 2017. Anthelmintic activity of cytochrome P450 inhibitors miconazole and clotrimazole: in-vitro effect on the liver fluke *Opisthorchis felineus*. Int. J. Antimicrob. Agents 50, 97–100.
Padthaisong, S., Thanee, M., Techasen, A., Namwat, N., Yongvanit, P., Liwatthakun, A., Hankla, K., Sangkhamanon, S., Loilome, W., 2017. Nimotuzumab inhibits cholangiocarcinoma cell metastasis via suppression of the epithelial-mesenchymal transition process. Anticancer. Res. 37, 3591–3597.
Pakharukova, M.Y., Correia da Costa, J.M., Mordvinov, V.A., 2019a. The liver fluke Opisthorchis felineus as a group III or group I carcinogen. 4open. 2, 23.
Pakharukova, M.Y., Ershov, N.I., Vorontsova, E.V., Katokhin, A.V., Merkulova, T.I., Mordvinov, V.A., 2012. Cytochrome P450 in fluke *Opisthorchis felineus*: Identification and characterization. Mol. Biochem. Parasitol. 181, 190–194.
Pakharukova, M.Y., Mordvinov, V.A., 2016. The liver fluke *Opisthorchis felineus*: biology, epidemiology, and carcinogenic potential. Trans. R. Soc. Trop. Med. Hyg. 110, 28–36.
Pakharukova, M.Y., Pakharukov, Y.V., Mordvinov, V.A., 2018. Effects of miconazole/clotrimazole and praziquantel combinations against the liver fluke *Opisthorchis felineus in vivo* and *in vitro*. Parasitol. Res. 117, 2327–2331.
Pakharukova, M.Y., Samsonov, V.A., Serbina, E.A., Mordvinov, V.A., 2019b. A study of tribendimidine effects *in vitro* and *in vivo* on the liver fluke *Opisthorchis felineus*. Parasit. Vectors 12, 23.
Pakharukova, M.Y., Vavilin, V.A., Sripa, B., Laha, T., Brindley, P.J., Mordvinov, V.A., 2015. Functional analysis of the unique cytochrome P450 of the liver fluke *Opisthorchis felineus*. PLoS. Negl. Trop. Dis. 9, e0004258.
Pakharukova, M.Y., Zaparina, O.G., Kapushchak, Y.K., Baginskaya, N.V., Mordvinov, V.A., 2019c. *Opisthorchis felineus* infection provokes time-dependent accumulation of oxidative hepatobiliary lesions in the injured hamster liver. PLoS ONE 14, e0216757.
Petrenko, V.A., Pakharukova, M.Y., Kovner, A.V., Lvova, M.N., Lyakhovich, V.V., Mordvinov, V.A., 2017. Secretion of thioredoxin peroxidase protein of cat liver fluke *Opisthorchis felineus* during modeling of experimental opisthorchiasis. Bull. Exp. Biol. Med. 162, 773–776.
Pomaznoy, M.Y., Logacheva, M.D., Young, N.D., Penin, A.A., Ershov, N.I., Katokhin, A.V., Mordvinov, V.A., 2016. Whole transcriptome profiling of adult and infective stages of the trematode *Opisthorchis felineus*. Parasitol. Int. 65, 12–19.
Razumov, I.A., Pomaznoy, M.Y., Belavin, P.A., Ponomareva, E.P., Mordvinov, V.A., 2016. Cloning of 28 kDa glutathione-s-transferase of the trematode *Opisthorchis felineus* and estimation of antigenic properties of recombinant protein. Parazitologiia 50, 82–91.
Sommer, A., Rickert, R., Fischer, P., Steinhart, H., Walter, R.D., Liebau, E., 2003. A dominant role for extracellular glutathione S-transferase from *Onchocerca volvulus* is the production of prostaglandin D2. Infect. Immun. 71, 3603–3606.
Sripa, B., Brindley, P.J., Mulvenna, J., Laha, T., Smout, M.J., Mairiang, E., Bethony, J.M., Loukas, A., 2012. The tumorigenic liver fluke *Opisthorchis viverrini* multiple pathways to cancer. Trends Parasitol. 28, 395–407.
Sripa, B., Kaewkes, S., Sithithaworn, P., Mairiang, E., Laha, T., Smout, M., Pairojkul, C., Bhudhisawasdi, V., Tesana, S., Thinkamrop, B., Bethony, J.M., Loukas, A., Brindley, P.J., 2007. Liver fluke induces cholangiocarcinoma. PLoS Med. 4, e201.
Sripa, B., Tangkawattana, S., Brindley, P.J., 2018. Update on pathogenesis of opisthorchiasis and cholangiocarcinoma. Adv. Parasitol. 102, 97–113. https://doi.org/10.1016/bs.apar.2018.10.001.
Strube, C., Buschbaum, S., Wolken, S., Schnieder, T., 2008. Evaluation of reference genes for quantitative real-time PCR to investigate protein disulfide isomerase transcription pattern in the bovine lungworm *Dictyocaulus viviparus*. Gene 425, 36–43.
Van Hoosier, G.L., McPherson, C.W., 1987. Laboratory Hamsters. Academic Press, Orlando.
World Health Organization (WHO), 2014. "Top Ten" list of food-borne parasites released. Food and Agriculture Organization of the United Nations/World Health Organization (FAO/WHO). Geneva. http://www.fao.org/news/story/en/item/237323/icode/ Accessed 23 January 2019.
Widlund, A.L., Baur, J.A., Vang, O., 2013. mTOR: more targets of resveratrol?. Expert Rev. Mol. Med. 15, e10.
Xiao, Z., Chen, C., Meng, T., Zhang, W., Zhou, Q., 2016. Resveratrol attenuates renal injury and fibrosis by inhibiting transforming growth factor-β pathway on matrix metalloproteinase 7. Exp. Biol. Med. (Maywood) 241, 140–146.
Yazdani, S., Bansal, R., Prakash, J., 2017. Drug targeting to myofibroblasts: Implications for fibrosis and cancer. Adv. Drug. Deliv. Rev. 121, 101–116.
Yongvanit, P., Pinlaor, S., Bartsch, H., 2012. Oxidative and nitrative DNA damage: key events in opisthorchiasis-induced carcinogenesis. Parasitol. Int. 61, 130–135.
Zen, Y., Adsay, N.V., Bardadin, K., Colombari, R., Ferrell, L., Haga, H., Hong, S.M., Hytiroglou, P., Klöppel, G., Lauwers, G.Y., van Leeuwen, D.J., Notohara, K., Oshima, K., Quaglia, A., Sasaki, M., Sessa, F., Suriawinata, A., Tsui, W., Atomi, Y., Nakanuma, Y., 2007. Biliary intraepithelial neoplasia: an international interobserver agreement study and proposal for diagnostic criteria. Mod. Pathol. 20, 701–709.